NRC Research Press

ARTICLE

Remote sensing evaluation of High Arctic wetland depletion following permafrost disturbance by thermo-erosion gullying processes[1]

Naïm Perreault, Esther Lévesque, Daniel Fortier, Denis Gratton, and Laurent J. Lamarque

Abstract: Northern wetlands and their productive tundra vegetation are of prime importance for Arctic wildlife by providing high-quality forage and breeding habitats. However, many wetlands are becoming drier as a function of climate-induced permafrost degradation. This phenomenon is notably the case in cold, ice-rich permafrost regions such as Bylot Island, Nunavut, where degradation of ice wedges and thermo-erosion gullying have already occurred throughout the polygon-patterned landscape resulting in a progressive shift from wet to mesic tundra vegetation within a decade. This study reports on the application of the normalized difference vegetation index to determine the extent of permafrost ecosystem disturbance on wetlands adjacent to thermo-erosion gullies. The analysis of a GeoEye-1 image of the Qarlikturvik valley, yielding a classification with five classes and 62% accuracy, resulted in directly identifying affected areas when compared to undisturbed baseline of wet and mesic plant communities. The total wetland area lost by drainage around the three studied gullies approximated to 95 430 m^2, which already represents 0.5% of the total wetland area of the valley. This is worrisome considering that 36 gullies have been documented in a single valley since 1999 and that permafrost degradation by thermal erosion gullying is significantly altering landscape morphology, modifying wetland hydrology, and generating new fluxes of nutrients, sediments, and carbon in the watershed. This study demonstrates that remote sensing provides an effective means for monitoring spatially and temporally the impact of permafrost disturbance on Arctic wetland stability.

Key words: Arctic wetlands, thermo-erosion gullies, permafrost disturbance, remote sensing, normalized difference vegetation index (NDVI).

Résumé : Les terres humides du Nord ainsi que leur végétation de toundra fertile sont d'une grande importance pour la faune arctique en procurant un fourrage de grande qualité et des habitats de reproduction. Cependant, beaucoup de terres humides deviennent plus sèches en fonction de la dégradation du pergélisol d'origine climatique. Ce phénomène est notamment le cas dans les régions de pergélisol froides, riches en glace comme l'île Bylot, Nunavut, où les phénomènes de fonte de coins de glace et de ravinement par érosion

Received 21 October 2016. Accepted 23 March 2017.

N. Perreault, E. Lévesque, and L.J. Lamarque. Département des Sciences de l'environnement, Université du Québec à Trois-Rivières, Trois-Rivières, QC G9A 5H7, Canada; Centre d'études nordiques, Université Laval, Québec, QC G1V 0A6, Canada.
D. Fortier. Centre d'études nordiques, Université Laval, Québec, QC G1V 0A6, Canada; Département de géographie, Université de Montréal, Montréal, QC H2V 2B8, Canada.
D. Gratton. Département des Sciences de l'environnement, Université du Québec à Trois-Rivières, Trois-Rivières, QC G9A 5H7, Canada.
Corresponding authors: Laurent J. Lamarque (e-mail: llamarqueab@gmail.com) and Esther Lévesque (e-mail: Esther.Levesque@uqtr.ca).
[1]This article is part of a Special issue entitled "Arctic permafrost systems".

thermique se sont déjà produits partout dans le paysage de polygones en plan, entraînant un changement progressif de la végétation de toundra humide à mésique en une décennie. Cette étude fait état de l'application d'indice de végétation par différence normalisée afin de déterminer l'ampleur de la perturbation des écosystèmes du pergélisol affectant les terres humides adjacentes aux ravins d'érosion thermique. L'analyse d'une image de GeoEye-1 de la vallée Qarlikturvik, rapportant une classification à cinq classes avec une exactitude de 62%, a permis de directement identifier les zones touchées lorsque comparées à la référence, soit les communautés intactes de plantes humides et mésiques. La zone de terres humides totale perdue par le drainage autour des trois ravins étudiés était approximativement 95 430 m2, ce qui représente déjà 0,5% de la zone de terres humides totale de la vallée. Ceci est inquiétant étant donné que 36 ravins ont été documentés dans une seule vallée depuis 1999 et cette dégradation du pergélisol par ravinement d'érosion thermique change significativement la morphologie du paysage, modifie l'hydrologie des terres humides et produit de nouveaux flux de nutriments, de sédiments et de carbone dans le bassin hydrographique. Cette étude démontre que la télédétection est un moyen efficace de surveiller dans le temps et dans l'espace les effets de perturbation du pergélisol sur la stabilité des terres humides arctiques.

Mots-clés : terres humides de l'Arctique, ravins formés par érosion thermique, perturbation du pergélisol, télédétection, indice de végétation par différence normalisée (NDVI).

Introduction

Wetlands, accounting for up to 80% of the total surface area in some Arctic regions (Pienitz et al. 2008; Rautio et al. 2011), represent prominent ecosystems for tundra biodiversity and livelihood of local communities. They offer critical staging and nesting homes to many birds (Hughes et al. 1994; Lepage et al. 1998; CAFF 2013) and provide many herbivores refuges from predators and preferred grazing grounds with abundant graminoid species (Henry 1998; Kristensen et al. 2011; Doiron et al. 2014). Northern wetlands also play a significant role in global gas exchanges by storing large quantities of carbon due to slow organic matter decomposition rates (Tarnocai et al. 2009; Hugelius et al. 2014; Bouchard et al. 2015) and by producing 5%–20% of total natural methane emissions to the atmosphere (Olefeldt et al. 2013; McEwing et al. 2015).

Northern wetlands are highly sensitive to current climate warming. Their sustainability relies on the integrity of perennially frozen ground that provides permanent or seasonal water supply and prevents vertical percolation (Woo 2012; Natali et al. 2015). However, observations over the last decades indicate that permafrost thawing and active layer deepening, closely related to the ratio of ground ice content and ground thermal conditions (Burn and Kokelj 2009; Kanevskiy et al. 2013; Rudy et al. 2017), have intensified with increasing temperatures (Romanovsky et al. 2010; Rowland et al. 2010; Liljedahl et al. 2016; Vincent et al. 2017). The resulting changes in hydrological conditions can have profound consequences for biochemical cycles and ecological communities (see Wrona et al. 2016 for a review). The rapid development of new drainage channels may for instance reduce the areal extent of wetlands globally (Klein et al. 2005; Fortier et al. 2007; Avis et al. 2011; Godin and Fortier 2012*a*).

Continuous permafrost zones with widespread ice-wedge networks are particularly prone to instability given the large amount of ice found near the top of permafrost (Jorgenson et al. 2006; Kanevskiy et al. 2013; Liljedahl et al. 2016), and wetlands in these regions are highly susceptible to thermo-erosion gullying (Kokelj and Jorgenson 2013; Kokelj et al. 2014). This permafrost geosystem feature results from thermal and mechanical degredation of ice wedges subsequent to ice melt through convective heat flow between running water and ice/frozen ground (Fortier et al. 2007; Morgenstern et al. 2013; Godin 2016). Thermo-erosion gullying has been reported from many sites throughout the circumpolar North and the Antarctic (Levy et al. 2008; Grosse et al. 2011; Günther et al. 2013; Liljedahl et al. 2016). On Bylot Island, Nunavut, thermo-erosion processes led to substantial permafrost tunneling, gullying, and subsequent mass wasting with an eroded area estimated at nearly

158 000 m^2 within 10–15 years after gully inception (Fortier et al. 2007; Godin and Fortier 2012*a*; Godin et al. 2014; Veillette et al. 2015). In consequence, adjacent wetlands were severely affected by rapid drainage. The decrease in soil moisture and thaw-front depth in disturbed low-centered polygons culminated in a relatively rapid transition from wet to mesic plant communities (Godin et al. 2016; Perreault et al. 2016).

Satellite data have been used increasingly in the Arctic for various geomorphological purposes such as mapping polygonal tundra landscape components (Skurikhin et al. 2013), detecting degradation of ice wedges (Liljedahl et al. 2016), assessing permafrost coast erosion (Obu et al. 2016), understanding effects of flooding following storm (Lantz et al. 2015), and monitoring permafrost thaw dynamics (Ulrich et al. 2014; Beck et al. 2015; Günther et al. 2015; Liu et al. 2015; Saruulzaya et al. 2016). Techniques such as InSAR (interferometric synthetic aperture radar) as well as airbone and terrestrial laser scanning have been used to document detailed topographical changes (Chen et al. 2013; Hubbard et al. 2013; Liu et al. 2014; Wolfe et al. 2014), thermokarst (Barnhart and Crosby 2013), active layer thickness (Gangodagamage et al. 2014; Schaefer et al. 2015; Widhalm et al. 2017), and freeze–thaw cycles (Daout et al. 2017). While remote sensing studies have also characterized the distribution of thermo-erosion landforms (Morgenstern 2012; Belshe et al. 2013; Godin et al. 2014), they have yet to examine the impacts of these processes on surrounding vegetation. Using the satellite-derived normalized difference vegetation index (NDVI) coupled with field surveys of plant community composition, our objective was to test the feasibility of remotely sensed data for quantitatively assessing the extent of landscape-scale permafrost disturbance on the depletion of adjacent wetlands.

Materials and methods

Study area

This work was conducted in the Qarlikturvik valley on Bylot Island, Nunavut, Canada (73°09′N, 79°57′W) (Fig. 1). Located on the southern plain of the island, which is part of the Sirmilik National Park, the valley has a surface area of 75 km^2 and is ~17 km long and 4–5 km wide. It is bounded to the north and south by plateaus (~500 m a.s.l.) and to the east by the C-79 and C-93 glaciers (Inland Waters Branch 1969). A proglacial river runs in a glaciofluvial outwash plain through braided channels that prograde into the Navy Board Inlet to the west forming a wide delta. Streams and rills coming from subperpendicular valleys and from alluvial fans can be temporarily connected to the river. The plain is bordered on both sides by low-gradient terraces that have developed as the accumulation of ~4–5 m of ice-rich peat mixed with aeolian and alluvial silts and sands following glacier retreat during the Holocene (Fortier and Allard 2004; Fortier et al. 2006). Networks of syngenetic ice wedges formed during the Late Holocene and resulted in the development of a polygonal-patterned ground that features high- and low-centered polygons, polygon ponds, and thaw lakes (Hughes et al. 1994; Fortier and Allard 2004; Bouchard et al. 2015). In this area, mean air temperature averaged −14.7 °C at 24 m a.s.l. for the 1995–2015 period (CEN 2016). Spring and fall temperatures have risen by 2.8 and 4.3 °C, respectively, over the past 35 years (Gauthier et al. 2011), while the annual cumulative number of thawing degree-days has increased from 381 in 1989 to 521 in 2011 (Gauthier et al. 2013).

Site characteristics

Our study sites were located within the low-centered polygon landscape. These ice-wedge polygons are 10–20 m across with well-developed ridges 2–6 m wide. The landscape is generally characterized by two baseline plant communities: (1) wetlands, supported by snowmelt water from surrounding hills and dominated by sedges (*Carex aquatilis* Wahlenb., *Eriophorum angustifolium* Honk., *Eriophorum scheuchzeri* Hoppe), grasses (*Dupontia fisheri* R. Br.,

Fig. 1. Location of the study area. (*a*) The Qarlikturvik valley (circle), Bylot Island (rectangle), Nunavut, Canada. (*b*) False color GeoEye-1 image of the valley (taken on September 2, 2010, at 17:40 GMT) and the three studied thermo-erosion gullies located on syngenetic ice-wedge polygon terraces (IWPT) bordering a glacio-fluvial outwash plain, terminating in a delta prograding into Navy Board Inlet.

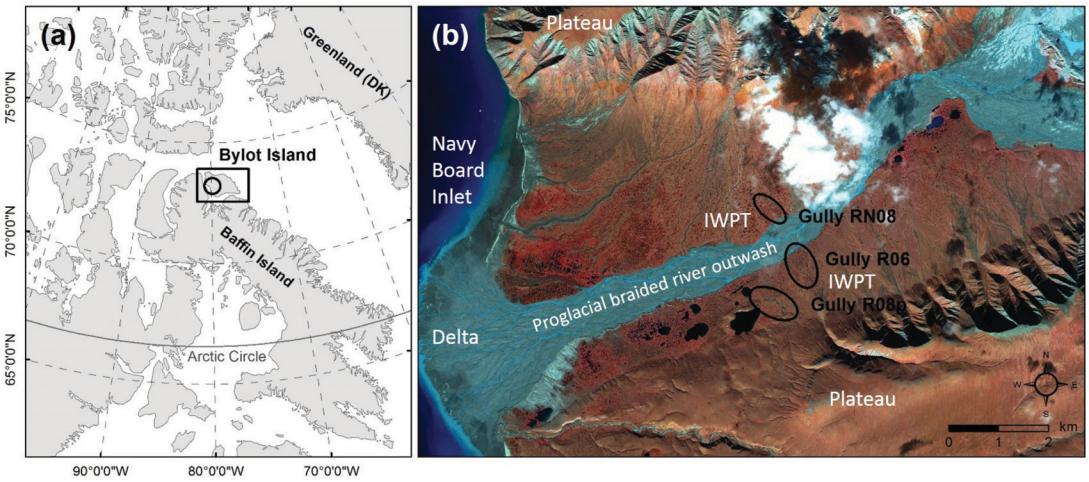

Pleuropogon sabinei R. Br.; Gauthier et al. 1995), and fen mosses (*Drepanocladus* spp.; Pouliot et al. 2009), and (2) mesic environments, characterized by better drained soils and located on polygon rims, sloping terrain, and hummocky tundra, which are colonized by mesic species such as *Salix* spp., *Vaccinium uliginosum* L., *Arctagrostis latifolia* (R. Br.) Griseb., *Poa arctica* R. Br., *Luzula confusa* Lindeberg, and *Aulocomnium* spp. (Zoltai et al. 1983; Duclos 2002; Audet et al. 2007).

Field surveys were specifically conducted around three gullies that were selected among the 36 reported by Godin and Fortier (2012*a*) in the low-centered polygon landscape (Figs. 1*b* and 2). These gully networks, closely monitored since 1999, originated from the collapse of underground tunnels that followed the infiltration of snowmelt water into cavities formed in the frozen active layer and permafrost (Fortier et al. 2007; Godin and Fortier 2010). The gullies R08p and R06, respectively 805 and 717 m long, were characterized by ongoing thermal erosion, while the gully RN08, 180 m long, has been very weakly active in recent years (Godin and Fortier 2012*a*; Veillette et al. 2015). Vegetation surveys were carried out during the 2009 and 2010 plant growing seasons at 197 sampling sites (n = 95, 81, and 21 around gullies R08p, R06, and RN08, respectively), which were selected using a stratified random sampling design to encompass intact wet and mesic sites as well as disturbed polygons (n = 62, 48, and 87 for wet polygons, mesic environments, and disturbed polygons, respectively) (see Perreault (2012) and Perreault et al. (2016) for a detailed description of the methods and habitats). The position of each sampling site was recorded using a 5 m accuracy GPS receiver (Garmin eTrex Venture HC). Plant species richness was highest in disturbed polygons where species of wet polygons and mesic environments were present (total species richness = 36, 47, and 54 in wet polygons, mesic environments, and disturbed polygons, respectively). Species abundance in disturbed polygons represented a middle-range state between wet and mesic conditions and were thus covered by both hydrophilic species such as *Carex aquatilis* and *Dupontia fisheri* and mesic species such as *Salix arctica* and *Arctagrostis latifolia* (Table 1). The moss carpet was mainly made of living *Drepanocladus* spp. in wet polygons, living *Aulocomnium* spp. in mesic environments, and dried (i.e., dead) species in disturbed polygons (Table 1).

Fig. 2. Oblique aerial views of the three thermo-erosion gullies studied in the Qarlikturvik valley, Bylot Island, Nunavut (photographs taken on July 23, 2013, by D. Fortier): (*a*) gully R08p (805 m long), (*b*) gully R06 (717 m long), and (*c*) gully RN08 (180 m long). Each ice-wedge polygon located along the gullies is approximately 15–20 m wide. The gullies follow closely the network of ice wedges in the ground, which explains the angularity of the gully channels. The widths of the gully cross-sections vary along their length but generally range from 2 to 20 m. The depths of the gully cross-sections are a function of the base level of the gully channel at the gully outlet. The depths increase upstream according to the topographic gradient of the terrace to reach over 4 m at the gully head. The arrows indicate the general water flow direction.

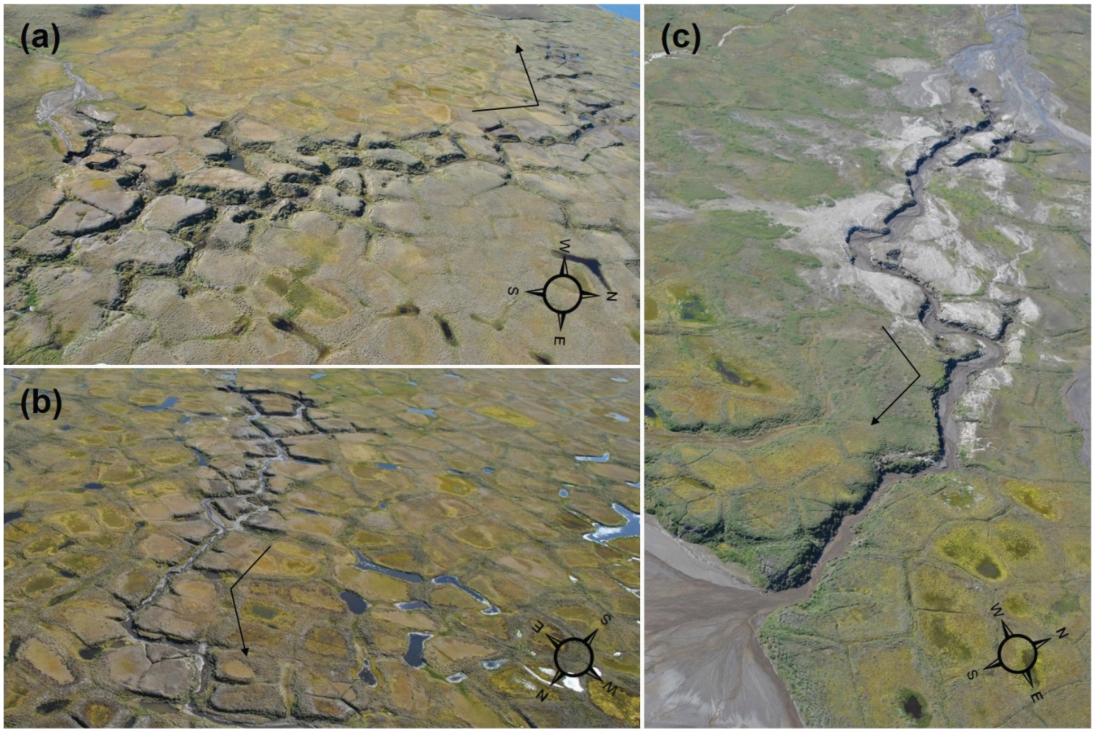

Remote sensing data analysis

We used a high-resolution satellite image of the Qarlikturvik valley acquired by the GeoEye sensor (GeoEye Inc., Herndon, Virginia) on September 2, 2010, at 17:40 GMT. This sensor covered an area of 14 km long × 19 km wide with a 0.5 m spatial resolution panchromatic band and four multispectral bands between 450 and 920 nm of 2 m spatial resolution (GeoEye Elevating Insight, GeoEye Inc.). The sun elevation and azimuth angles at the time of image acquisition were 24.37° and 185.86°, respectively, whilst the sensor look angle and elevation were 81.40° and 220.18°, respectively. Cloud cover represented less than 5% of the scene. The image was delivered geometrically corrected in UTM coordinates (Zone 17 N in the world geodetic system, WGS 84).

Image analysis

Image processing and spatial data analyses were conducted using the ENVI image analysis (Exelis Geospatial Systems, Rochester, New York and the ArcGIS version 9.2 (Esri, Redlands, California) software packages. We first preprocessed the satellite image by applying a geographical correction based on the differential global positioning system (DGPS) coordinates of the studied gullies (Godin and Fortier 2010, 2012*a*, 2012*b*) and by converting the raw digital numbers of red and near-infrared bands to Top Of Atmosphere (TOA) reflectance values (Goward et al. 2003). Following cloud masking, a subset scene of the valley

Table 1. Mean cover (%) of the most commun taxa present in the three types of habitat (wet polygons, mesic environments, and disturbed polygons) studied along thermo-erosion gullies in the Qarlikturvik valley, Bylot Island, Nunavut (modified from Perreault et al. 2016).

	Habitat		
	Wet polygons (n = 62)	Mesic environments (n = 48)	Disturbed polygons (n = 87)
Vascular taxa			
Cyperaceae			
Carex aquatilis	14.7	1.9	12.1
Eriophorum angustifolium	0.5	0	0.5
Eriophorum scheuchzeri	2.1	<	0.2
Juncaceae			
Luzula arctica	<<	1.0	0.2
Luzula confusa	<	2.0	1.5
Poaceae			
Anthoxanthum arcticum	0.5	<<	<<
Arctagrostis latifolia	0.6	3.0	0.2
Dupontia fisheri	7.4	0.1	3.3
Festuca brachyphylla	<<	<	0.2
Salicaceae			
Salix arctica	1.2	10.8	2.0
Salix herbacea	0	0.1	<
Salix reticulata	<<	1.6	0.1
Salix richardsonii	<<	<<	<<
Nonvascular taxa			
Lichens	<	6.6	1.0
Live mosses	53.1	44.6	21.3
Drepanocladus spp.	39.9	0	13.3
Aulocomnium spp.	7.5	39.3	2.3
Dried mosses	2.5	0.9	24.0
Total live vascular plant cover	28.1	21.3	22.6
Total live plant cover	81.3	72.6	44.4
Total plant cover	83.8	73.5	68.4

Note: <<, cover <0.01%; <, cover <0.1%. Total covers (%) of both common and rare taxa are also indicated.

encompassing areas of interest was obtained by manually digitizing boundaries. Spectral bands were merged with the panchromatic image to create 0.5 m standard pan-sharpened multispectral images, i.e., true and false color composite images. This step ensured the accurate positioning of sampling sites, as gully and sampling site GPS positions were projected onto the GeoEye satellite image. Analysis areas — one per sampling site — were identified following the thorough description of plant communities and environmental conditions from Perreault et al. (2016). Each analysis area, which excluded polygon rims, incorporated as many pixels as possible (2 m × 2 m per pixel) in order to have a good representation of its corresponding sampling site. A minimum of 6 pixels was integrated per analysis area for a total of 5406 selected pixels (1832 pixels for wet polygons, 931 pixels for mesic environments, and 2643 pixels for disturbed polygons). Analysis areas were finally digitized as Regions Of Interest (ROI) in ENVI and used to create NDVI values for each habitat type (i.e., for wet polygons, mesic environments, and disturbed polygons) (Fig. 3).

NDVI calculation

The NDVI was determined as follows: NDVI = $(P_{nir} - P_{red})/(P_{nir} + P_{red})$, where P_{nir} and P_{red} respectively represent the spectral reflectance in the near-infrared (from the plant canopy)

Fig. 3. Location of the 197 analysis areas around (*a*) gully R08p, (*b*) gully R06, and (*c*) gully RN08 (wet polygons (n = 62), mesic environments (n = 48), disturbed polygons (n = 87)). The types of habitat were characterized by geomorphological and vegetation field surveys, while the size of each site was estimated via image analysis.

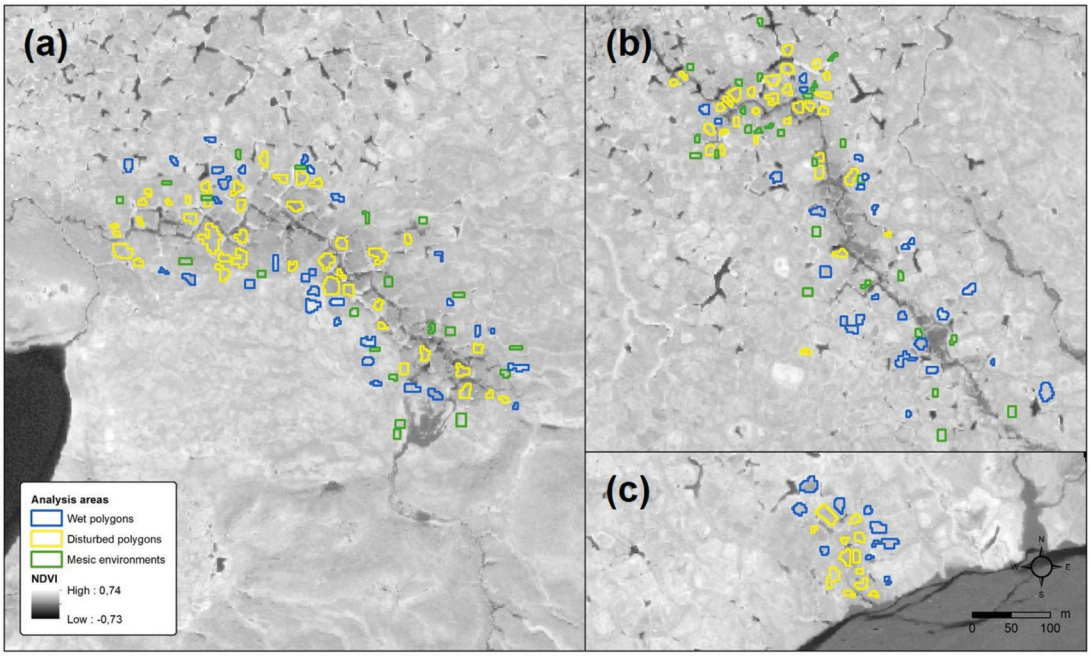

and in the red (where chlorophyll absorbance is maximal) (Raynolds et al. 2008). This global vegetation index, which measures the vegetation relative greenness, yields values between −1 and 1, with those close to −1 representing areas devoid of vegetation and those close to 1 referring to dense vegetation areas (Rouse et al. 1973; Tucker and Sellers 1986; Pettorelli 2013). A proportionate stratified random sampling method (by vegetation class) was used to select 80% of the analyzed pixels. NDVI statistics (means, medians, quartiles, and percentiles) were calculated for each type of habitat based on this selection.

Image classification and mapping of affected areas

A simple threshold-based classification technique was performed on the NDVI image to determine class thresholds, using the 80% of the analysis area pixels that were selected beforehand. The residual 20% were used to assess the accuracy of the classification. A standard confusion matrix was used to assess the accuracy between class thresholds and habitat types. Before the majority filter was applied, we calculated the overall accuracy (i.e., the proportion of correctly classified pixels) for the classified image and the Kappa coefficient, which indicates the percentage of correctly allocated pixels (Thomas et al. 2003; Congalton and Green 2009). Because data following pixel-based classification show so-called salt–pepper noise (Rongqun and Daolin 2011), a 3 pixel × 3 pixel majority filter was applied to the classified image to improve type unification. Low-NDVI areas located around the gullies were vectorized considering 8 adjacent pixels for the connectivity and a minimum of 20 pixels per region. Vectorized images were exported to ArcGIS and these areas surrounding gullies were retained for the determination of disturbed areas. For this study, the contours of the gullies were mapped using the gully cartography from Godin and Fortier (2010, 2012*a*).

Results

Remote sensing data analysis

Habitat NDVI

The NDVI analysis emphasized a marked difference between undisturbed sites — from either wet or mesic environments — and disturbed areas, with greater NDVI values for wet polygons and mesic environments compared to disturbed polygons (Fig. 4). The NDVI value of 0.27, which corresponded to both the lower quartile of mesic environments and the upper quartile of the disturbed polygons, separated the greater vegetation cover of wet and mesic sites from the lower vegetation cover of disturbed areas. There was a strong overlap in NDVI values between wet and mesic sites, and the NDVI value of 0.33, corresponding to the median of wet polygons and the upper quartile of mesic environments, was used to differentiate these two baseline habitats.

Image classification

The NDVI values ranged from −0.73 to 0.74 for the processed scene (Fig. 5). The final satellite-derived NDVI image was classified into five classes with the last three related to the habitat types of interest: (1) class 1 (−0.73 to −0.1) represented water bodies, (2) class 2 (−0.1 to 0.15) represented bare grounds such as proglacial braided river bars and aeolian sand covers, (3) class 3 (0.15–0.27) represented areas poorly covered by vegetation surrounding alluvial fans and drainage systems, and (4) classes 4 (0.27–0.33) and 5 (0.33–0.74) were associated with mesic and wet environments, respectively (Table 2). The classification was supported by an overall accuracy of 61.7% and a Kappa coefficient of 0.41. When wet polygons and mesic environments were pooled together, the overall accuracy increased to 79.5% with a Kappa coefficient of 0.59, providing another evidence of the similarity in NDVI trends between these two types of habitats.

Mapping of affected areas

In the three studied cases of thermo-erosion gullying and subsequent permafrost mass wasting and wetland drainage, disturbed areas were directly adjacent to new drainage systems formed by the gullies and distributed all along their length on both sides of gully channels (Fig. 6). Nearby sites had higher NDVI values, highlighting the dominance of wet polygons and mesic environments (Fig. 5). The overall wetland area affected by the three gullies was approximately 95 430 m^2, corresponding to 56 m^2 of disturbed area per linear metre of gullying. Considering that wetlands cover 34% of the Qarlikturvik valley total area (19 km^2 out of 56 km^2) (Massé 1998), thermo-erosion gullying along these three gullies only has drained 0.5% of the total wetland area within a decade. The extent of disturbed areas due to drainage strongly differed among gullies with the greatest disturbances found around the active R08p and R06 gullies (Table 3; Fig. 2).

Discussion

Having previously reported that the initiation of thermo-erosion gullying has led to the relatively rapid replacement of hydrophilic plant species by those indigenous to mesic environments (Perreault et al. 2016), we sought here to assess and quantify the extent of disturbed wetlands by permafrost disturbance using fine-scale remotely sensed data. Climate-driven changes to surface moisture and wind regimes at the century timescale have been documented for the study site over the Late Holocene (Fortier et al. 2006). However, drastic and rapid changes to surface wetness that are linked to the development of thermo-erosion gullies are unprecedented (Fortier et al. 2007; Godin et al. 2014) and may imply a fundamental change in the hydrological cycle in response to changing snowmelt

Fig. 4. For each type of habitat (WP, wet polygons; ME, mesic environments; DP, disturbed polygons), (*a*) NDVI values calculated based on 80% of the analysis area pixels (n = 1465 pixels from 62 sites for wet polygons, n = 745 pixels from 48 sites for mesic environments, n = 2127 pixels from 87 sites for disturbed polygons), the 10th percentile, lower quartile, median (standard line), mean (dash line), upper quartile, and 90th percentile are represented with the 5th and 95th percentiles shown as dots and the dotted line representing the difference between vegetation cover of wet and mesic sites and that of disturbed areas (NDVI value of 0.27) and (*b*) number of pixels at each NDVI value.

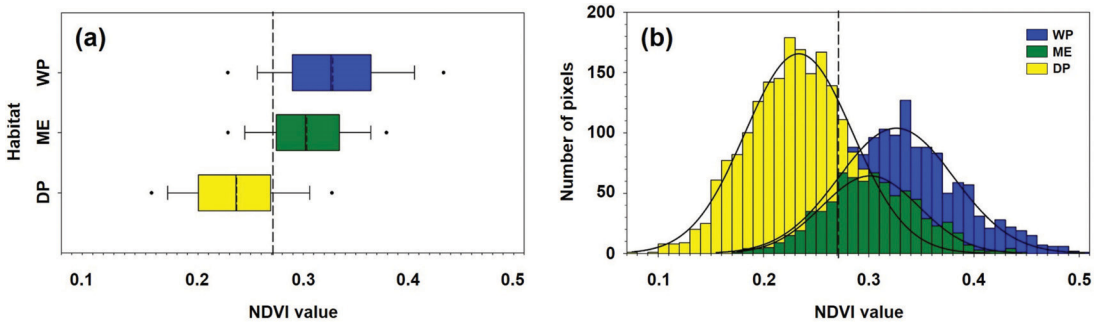

Fig. 5. GeoEye-1 NDVI image for the Qarlikturvik valley, Bylot Island, Nunavut. Classes 1 and 2 represent water bodies and bare ground, respectively, while classes 3–5 are related to the three studied habitat types, i.e., disturbed polygons (in yellow), mesic environments (in light green), and wet polygons (in dark green). IWPT refers to the ice-wedge polygon terraces.

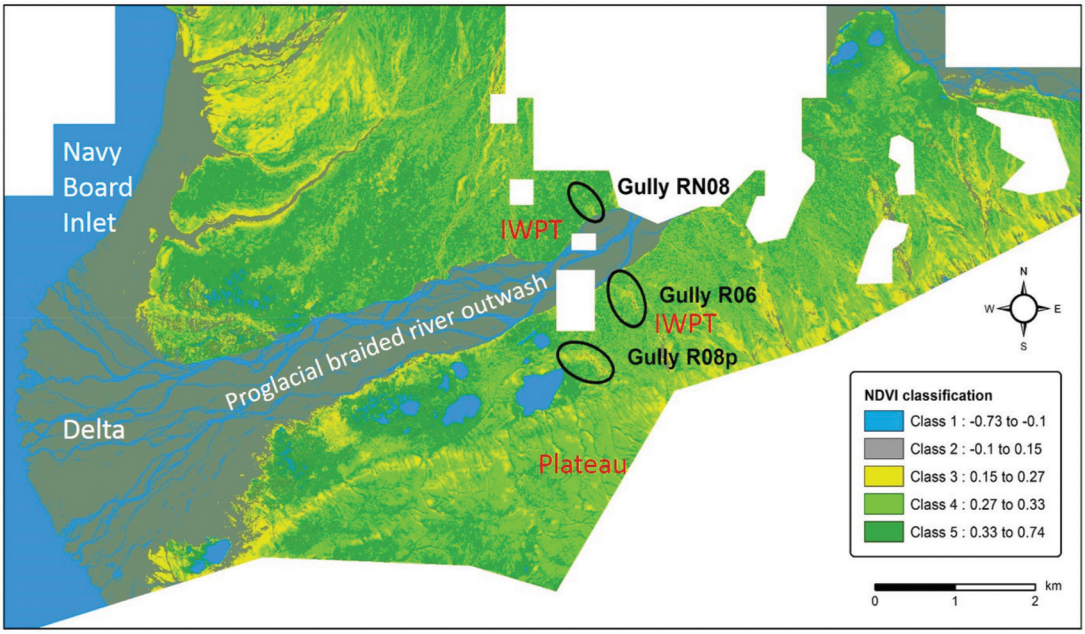

water runoff conditions. Using high-resolution NDVI may therefore help to understand the magnitude of change and to follow vegetation changes in time as the climate warms.

While NDVI values for wet and mesic sites overlapped significantly due to similar total live plant cover present in these habitats at the time the image was taken, the analysis we carried out from GeoEye data allowed for a good discrimination between disturbed and undisturbed wetland and mesic vegetation types. The areas affected by thermo-erosion processes were restricted to the gully edges, illustrating the strong control of ice-wedge

Table 2. Confusion matrix showing results of the classification accuracy.

	Habitat			
NDVI class	Wet polygons	Mesic environments	Disturbed polygons	Total number of pixels
% of selected pixels				
Class 3 (0.15–0.27)	14	20	75	250
Class 4 (0.27–0.33)	37	51	22	342
Class 5 (0.33–0.74)	49	29	3	477
Total number of pixels	367	186	516	1069

Note: Proportion (%) of residual pixels per NDVI class for each of the three habitat types (wet polygons, mesic environments, and disturbed polygons) encountered around thermo-erosion gullies in the Qarlikturvik valley, Bylot Island, Nunavut. NDVI classes 1 and 2 for which the analysis was not suitable are not shown.

Fig. 6. Extent of thermo-erosion impact along (*a*) gully R08p, (*b*) gully R06, and (*c*) gully RN08. Classes 1 and 2 represent water bodies and bare ground, while classes 3–5 are related to the three studied habitat types, i.e., disturbed polygons (in yellow), mesic environments (in light green), and wet polygons (in dark green). Disturbed areas were estimated via NDVI values derived from pseudo-color images. Hatched areas represent the gully topographic contours extracted from Godin and Fortier (2010, 2012*a*). Red lines outlining the yellow color of class 3 indicate the extent of the thermo-erosion-induced disturbed areas using both gully cartography from Godin and Fortier and the NDVI analyses. The arrows indicate the general water flow direction.

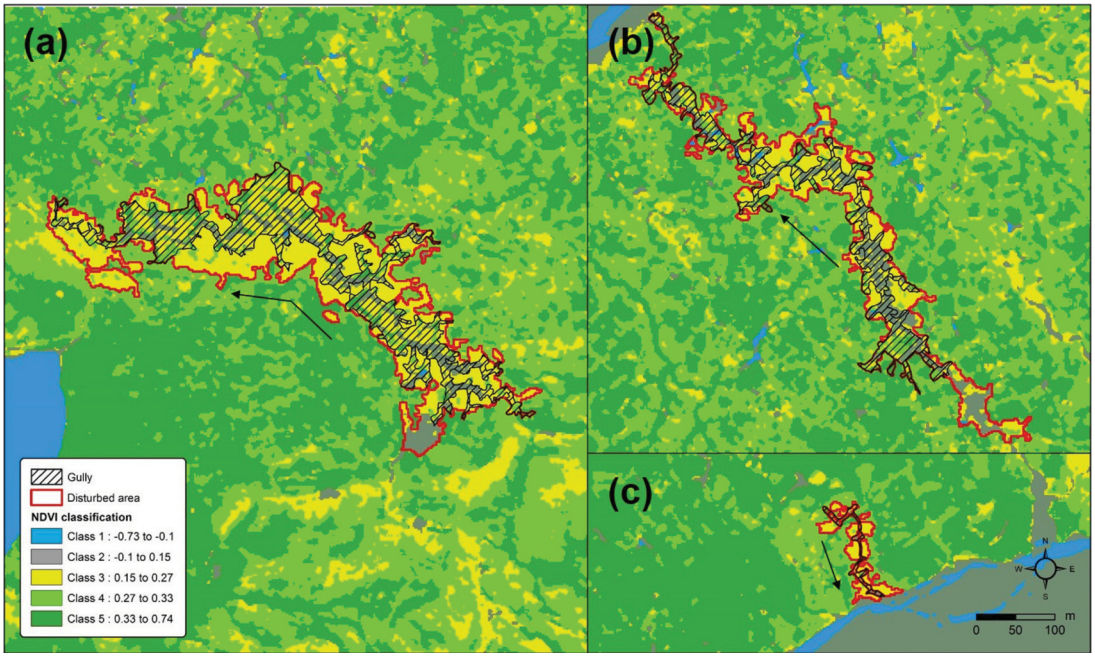

networks in shaping polygon landscape hydrology (Liljedahl et al. 2012, 2016; Vonk et al. 2013). Water drainage subsequent to thermo-erosion gullying has induced a significant decrease in soil moisture of disturbed polygons where wetland vegetation has not been able to persist and is being replaced by mesic plant species (Godin et al. 2016; Perreault et al. 2016). Considering that the stable state of mesic vegetation has not yet been reached, disturbed polygons currently encompass both wet and mesic plant species, with a total vascular plant cover similar to that in undisturbed sites (approximately 25%). The low NDVI characterizing these zones is therefore due to the higher proportion of dried mosses, as increases in NDVI values are tightly linked to the green moss layer thickness and moss water content (Douma et al. 2007; Engstrom et al. 2013).

Table 3. Extent of affected areas around the three studied gullies of the Qarlikturvik valley, Bylot Island, Nunavut.

			Area affected by drainage		Total disturbed area	
Gully	Gully length (m)	Gully area (m^2)	m^2	m^2 m $gully^{-1*}$	m^2	m^2 m of $gully^{-1*}$
R08p	805	27 762	31 018	39	58 780	73
R06	717	14 825	18 184	25	33 009	46
RN08	180	926	2 715	15	3 641	20
Total	1702	43 513	51 917	31	95 430	56

Note: Length and area of gullies R08p and R06 were retrieved from Godin and Fortier (2012*a*), while length of gully RN08 was measured using the GeoEye-1 panchromatic band and the measurement tool in ENVI. The asterisk refers to the ratio of affected areas and gully lengths.

The three studied gullies have already drained within 10 years approximately 95 000 m^2 of wetland areas, distributed along 1702 m of gullies. Such disturbance, which takes into consideration both the wetland drainage per se and the gully areas, that also represent a net loss of habitat since no stable vegetation has established to date, amounts to a loss of 0.5% of the total wetland area of the valley. With an average of 56 m^2 of affected area per linear metre of gullying, thermo-erosion-induced drainage of wetlands is worrisome for the near-future sustainability of these systems, especially since (1) R08p and R06 gullies have shown rapid thermo-erosion progression (i.e., 23 m $year^{-1}$) (Godin and Fortier 2012*a*) and (2) a total of 36 gullies have been characterized in the Qarlikturvik valley since 1999 for an overall eroded area already estimated at 158 000 m^2 (Godin and Fortier 2010, 2012*a*; Godin et al. 2014), corresponding to a net habitat loss of 0.8%. Thermo-erosion processes thus represent a major threat to wetland carrying capacity, which will be even more pronounced when accounting for the wetland areas depleted by drainage around all of the 36 gullies in the valley. Indeed, these wetlands support graminoids such as *Dupontia fisheri* and *Eriophorum scheuchzeri* that are preferred food resources of greater snow geese (Cadieux et al. 2008; Doiron et al. 2014). Between 1990 and 2012, snow geese, which can number up to 650 breeding pairs in the valley, consumed on average 30% of the above-ground biomass that was annually produced in the wetlands (Gauthier et al. 2013). Their nesting success may also be impacted by wetland depletion, as a decrease in water availability implies increased distances to water sources and therefore reduced ability to defend nests against predators such as the arctic fox (Lecomte et al. 2008). The rapid decrease of wetland habitats could also affect other tundra species (Berteaux et al. 2017); for example, the community structure of Arctic arthropods is strongly dependent, even at small spatial scales, on vegetation composition changes (Hansen et al. 2016). Although wetlands are common throughout the valley, it is worth noting that their distribution is heterogeneous; hence, the consequences of their depletion due to permafrost disturbance may be exacerbated in places where they are scarcer. Finally, thermo-erosion gullying is likely to alter greenhouse gas emissions at large scales. Methane emissions, which are strongly regulated by wetland habitats (Olefeldt et al. 2013; Tveit et al. 2015), may decrease as a result of adjacent wetland drainage. On the contrary, carbon release may increase given that wetlands generally act as carbon sinks (Bouchard et al. 2015; Treat et al. 2015), whilst the export of sediments via the gully channels would provide greater fluxes of particulate, dissolved carbon and nutrients (Godin et al. 2014).

The impact of thermo-erosion processes strongly varied between gullies. The greatest disturbances found along the R08p and R06 gullies can be explained by the substantial lengths of the main channels and the presence of secondary channels (Godin and Fortier 2012*b*). The R08p gully has been expanding simultaneously on six distinct secondary channels, while the R06 gully main channel progression has been among the fastest thermo-erosion development rates in the valley (Godin and Fortier 2012*a*). Comparatively, the

RN08 gully, which has not been active recently, is significantly shorter and does not have secondary axes (Godin and Fortier 2012*a*; Godin 2016). Given that these three gullies have all developed on peaty sandy to silty deposits, differences in erosion activity features among them may not be related to the sedimentary environments.

Satellite remote sensing data have played a prominent role in the observation and interpretation of spatial and temporal land cover changes over large spatial extents in the Arctic (Stow et al. 2004; Muster et al. 2013; Jorgenson and Grosse 2016; Park et al. 2016). As a result, NDVI analyses have been applied increasingly in studies of Arctic ecology for various purposes such as reporting climate-induced plant community composition changes (Rudy et al. 2013; Beck et al. 2015; Pattison et al. 2015), quantifying permafrost degradation (Fraser et al. 2011; Belshe et al. 2013), determining deglaciation effects on tundra vegetation distribution (Raynolds and Walker 2009), or predicting peaks of above-ground plant biomass (Doiron et al. 2013). In this study, undisturbed baseline wet and mesic communities were adequately separated from disturbed areas; hence, we suggest that finer spatial resolution analyses of NDVI trends can be effective for monitoring the drying or recovery of wetlands following inception of thermo-erosion gullying. This approach is likely to yield higher accuracy provided the satellite data are acquired earlier in the growing season, e.g., when wet polygons are more water-saturated, to better differentiate these two baseline vegetation types. Differences between vegetation types are indeed greater when NDVI is calculated around the peak growing season when there is maximum green leaf area (Riedel et al. 2005; Bratsch et al. 2016); however, in our case, satellite data were acquired at the end of summer when wet polygons and mesic environments show similar values of total above-ground biomass (50.5 ± 2.8 g m^{-2} in wetlands and 44.2 ± 6.8 g m^{-2} in mesic tundra) (Legagneux et al. 2012). Additional strategies to increase differentiation between nondisturbed wet and mesic vegetation communities may include considering plant structure and variations in soil moisture (Laidler and Treitz 2003; Laidler et al. 2008; Atkinson and Treitz 2012) as well as using other high-resolution remote sensing platforms. In this regard, unmanned aerial vehicles, which are relatively inexpensive and have successfully been tested for monitoring temporal dynamics of landslide and tundra vegetation (Turner et al. 2015; Fraser et al. 2016), as well as airborne laser scanning and interferometric synthetic aperture radar used to monitor topographic changes and active layer thickness (Gangodagamage et al. 2014; Liu et al. 2014; Schaefer et al. 2015; Widhalm et al. 2017) represent complementary techniques full of potential.

Conclusion

We found that the transformation of northern polygon landscapes and shifts in plant communities induced by thermo-erosion gullying processes can be accurately estimated by remotely sensed data. We presented a novel quantification of wetland disturbances that are induced by thermo-erosion gullying processes using fine-scale NDVI analyses. These results open up new opportunities to examine the causes of spatial heterogeneity in tundra response to warming. They will allow for the monitoring of the rapid changes associated with wetland disruption in the Arctic as well as for the evaluation of the contributions of permafrost degradation to global greenhouse gas emissions. This approach may also be useful for studying the long-term effects of slower hydrological regime changes on the transition between wet and mesic environments as well as for quantifying the feedbacks of vegetation succession on the stabilization of disturbed permafrost terrains.

Acknowledgements

We thank the Inuit community of Pond Inlet, Parks Canada-Sirmilik National Park, Centre d'études nordiques (CEN), and Dr. Gilles Gauthier (Université Laval) for facilitating access to Bylot Island field camp during summers 2009 and 2010. We are grateful to Alexandre Guertin-Pasquier and Etienne Godin for their assistance in the field and to the Polar Continental Shelf Program (Natural Resources Canada) for providing logistical support. This project was funded by the International Polar Year program of the Government of Canada, Fonds Québécois de la Recherche sur la Nature et les Technologies (FQRNT), Natural Sciences and Engineering Research Council of Canada (NSERC) Discovery Frontiers grant "Arctic Development and Adaptation to Permafrost in Transition" (ADAPT), NSERC Discovery grants to D. Fortier and E. Lévesque, the Network of Centers of Excellence of Canada ArcticNet, Northern Scientific Training Program (NSTP), the NSERC CREATE Training Program in Northern Environmental Sciences (EnviroNorth), the Groupe de Recherche en Biologie Végétale (GRBV) of Université du Québec à Trois-Rivières, and the Cold Regions Geomorphology and Geotechnical Laboratory (Geocryolab) of Université de Montréal.

References

Atkinson, D.M., and Treitz, P. 2012. Arctic ecological classifications derived from vegetation community and satellite spectral data. Remote Sens. **4**: 3948–3971. doi: 10.3390/rs4123948.

Audet, B., Lévesque, E., and Gauthier, G. 2007. Seasonal variation in plant nutritive quality for greater snow goose goslings in mesic tundra. Can. J. Bot. **85**: 457–462. doi: 10.1139/B07-039.

Avis, C.A., Weaver, A.J., and Meissner, K.J. 2011. Reduction in areal extent of high-latitude wetlands in response to permafrost thaw. Nat. Geosci. **4**: 444–448. doi: 10.1038/ngeo1160.

Barnhart, T.B., and Crosby, B.T. 2013. Comparing two methods of surface change detection on an evolving thermokarst using high temporal-frequency terrestrial laser scanning, Selawik River, Alaska. Remote Sens. **5**: 2813–2837. doi: 10.3390/rs5062813.

Beck, I., Ludwig, R., Bernier, M., Lévesque, E., and Boike, J. 2015. Assessing permafrost degradation and land cover changes (1986–2009) using remote sensing data over Umiujaq, sub-Arctic Québec. Permafrost Periglac. **26**: 129–141. doi: 10.1002/ppp.1839.

Belshe, E.F., Schuur, E.A.G., and Grosse, G. 2013. Quantification of upland thermokarst features with high resolution remote sensing. Environ. Res. Lett. **8**: 035016, doi: 10.1088/1748-9326/8/3/035016.

Berteaux, D., Gauthier, G., Domine, F., Ims, R.A., Lamoureux, S.F., Lévesque, E., and Yoccoz, N. 2017. Effects of changing permafrost and snow conditions on tundra wildlife: critical places and times. Arctic Sci. **3**: This issue. doi: 10.1139/as-2016-0023.

Bouchard, F., Laurion, I., Preskienis, V., Fortier, D., Xu, X., and Whiticar, M.J. 2015. Modern to millennium-old greenhouse gases emitted from freshwater ecosystems of the Eastern Canadian Arctic. Biogeosciences. **12**: 7279–7298. doi: 10.5194/bg-12-7279-2015.

Bratsch, S., Epstein, H.E., Buchborn, M., and Walker, D.A. 2016. Differentiating among four Arctic tundra plant communities at Ivotuk, Alaska using field spectroscopy. Remote Sens. **8**: 51, doi: 10.3390/rs8010051.

Burn, C.R., and Kokelj, S.V. 2009. The environment and permafrost of the Mackenzie Delta area. Permafrost Periglac. **20**: 83–105. doi: 10.1002/ppp.655.

Cadieux, M.-C., Gauthier, G., Gagnon, C.A., Lévesque, E., Bêty, J., and Berteaux, D. 2008. Monitoring the environmental and ecological impacts of climate change on Bylot Island, Sirmilik National Park. Université Laval, Québec, Qué.

CAFF (Conservation of Arctic Flora and Fauna). 2013. Arctic biodiversity assessment: synthesis. Akureyri, Iceland.

CEN. 2016. Climate station data from Bylot Island in Nunavut, Canada, v. 1.7 (1992–2016). Nordicana D2. doi: 10.5885/45039SL-EE76C1BDAADC4890.

Chen, F., Lin, H., Zhou, W., Hong, T., and Wang, G. 2013. Surface deformation detected by ALOS PALSAR small baseline SAR interferometry over permafrost environment of Beiluhe section, Tibet Plateau, China. Remote Sens. Environ. **138**: 10–18. doi: 10.1016/j.rse.2013.07.006.s.

Congalton, R.G., and Green, K. 2009. Assessing the accuracy of remotely sensed data: principles and practices. 2nd edn. CRC Press, Boca Raton, Fla.

Daout, S., Doin, M.-P., Peltzer, G., Socquet, A., and Lasserre, C. 2017. Large-scale InSAR monitoring of permafrost freeze–thaw cycles on the Tibetan Plateau. Geophys. Res. Lett. **44**: 901–909. doi: 10.1002/2016GL070781.

Doiron, M., Legagneux, P., Gauthier, G., and Lévesque, E. 2013. Broad-scale satellite normalized difference vegetation index data predict plant biomass and peak date of nitrogen concentration in Arctic tundra vegetation. Appl. Veg. Sci. **16**: 343–351. doi: 10.1111/j.1654-109X.2012.01219.x.

Doiron, M., Gauthier, G., and Lévesque, E. 2014. Effects of experimental warming on nitrogen concentration and biomass of forage plants for an arctic herbivore. J. Ecol. **102**: 508–517. doi: 10.1111/1365-2745.12213.

Douma, J.C., Van Wijk, M.T., Lang, S.I., and Shaver, G.R. 2007. The contribution of mosses to the carbon and water exchange of arctic ecosystems: quantification and relationships with system properties. Plant Cell Environ. **30**: 1205–1215. doi: 10.1111/j.1365-3040.2007.01697.x.

Duclos, I. 2002. Milieux mésiques et secs de l'Île Bylot, Nunavut (Canada): caractérisation et utilisation par la Grande Oie des Neiges. M.Sc. thesis, Université du Québec à Trois-Rivières, Trois-Rivières, Qué.

Engstrom, R., Hope, A., Kwon, H., and Stow, D. 2013. The relationship between soil moisture and NDVI near Barrow, Alaska. Phys. Geogr. **29**: 38–53. doi: 10.2747/0272-3646.29.1.38.

Fortier, D., and Allard, M. 2004. Late Holocene syngenetic ice-wedge polygons development, Bylot Island, Canadian Arctic Archipelago. Can. J. Earth Sci. **41**: 997–1012. doi: 10.1139/E04-031.

Fortier, D., Allard, M., and Pivot, F. 2006. A late-Holocene record of loess deposition in ice-wedge polygons reflecting wind activity and ground moisture conditions, Bylot Island, eastern Canadian Arctic. Holocene. **16**: 635–646. doi: 10.1191/0959683606hl960rp.

Fortier, D., Allard, M., and Shur, Y. 2007. Observation of rapid drainage system development by thermal erosion of ice wedges on Bylot Island, Canadian Arctic Archipelago. Permafrost Periglac. **18**: 229–243. doi: 10.1002/ppp.595.

Fraser, R.H., Olthof, I., Carriere, M., Deschamps, A., and Pouliot, D. 2011. Detecting long-term changes to vegetation in northern Canada using the Landsat satellite image archive. Environ. Res. Lett. **6**: 045502, pp. 9. doi: 10.1088/1748-9326/6/4/045502.

Fraser, R.H., Olthof, I., Lantz, T.C., and Schmitt, C. 2016. UAV photogrammetry for mapping vegetation in the Low Arctic. Arctic Sci. **2**: 79–102. doi: 10.1139/AS-2016-0008.

Gangodagamage, C., Rowland, J.C., Hubbard, S.S., Brumby, S.P., Liljedahl, A.K., Wainwright, H., Wilson, C.J., Altmann, G.L., Dafflon, B., and Peterson, U.C. 2014. Extrapolating active layer thickness measurements across Arctic polygonal terrain using LiDAR and NDVI data sets. Water Resour. Res. **50**: 6339–6357. doi: 10.1002/2013WR014283.

Gauthier, G., Hughes, R.J., Reed, R., Beaulieu, J., and Rochefort, L. 1995. Effect of grazing by greater snow geese on the production of graminoids at an arctic site (Bylot Island, NWT, Canada). J. Ecol. **83**: 653–664. doi: 10.2307/2261633.

Gauthier, G., Berteaux, D., Bêty, J., Tarroux, A., Therrien, J.-F., McKinnon, L., Legagneux, P., and Cadieux, M.-C. 2011. The tundra food web of Bylot Island in a changing climate and the role of exchanges between ecosystems. Ecoscience. **18**: 223–235. doi: 10.2980/18-3-3453.

Gauthier, G., Bêty, J., Cadieux, M.-C., Legagneux, P., Doiron, M., Chevallier, C., Lai, S., Tarroux, A., and Berteaux, D. 2013. Long-term monitoring at multiple trophic levels suggests heterogeneity in responses to climate change in the Canadian Arctic tundra. Philos. Trans. R. Soc. B. **368**: 20120482, pp. 12. doi: 10.1098/rstb.2012.0482.

Godin, E. 2016. Le processus de thermo-érosion du pergélisol dans la zone de pergélisol continu. Ph.D. thesis, Université de Montréal, Montréal, Qué.

Godin, E., and Fortier, D. 2010. Geomorphology of thermo-erosion gullies — case study from Bylot Island, Nunavut, Canada. *In* Proceedings, 6th Canadian Permafrost Conference and 63rd Canadian Geotechnical Conference, Calgary, Alta.

Godin, E., and Fortier, D. 2012*a*. Fine scale spatio-temporal monitoring of multiple thermo-erosion gullies development on Bylot Island, eastern canadian archipelago. *In* Proceedings, Tenth International Conference on Permafrost (TICOP), Salekhard, Russia. doi: 10.13140/2.1.3827.6803.

Godin, E., and Fortier, D. 2012*b*. Geomorphology of a thermo-erosion gully, Bylot Island, Nunavut, Canada. Can. J. Earth Sci. **49**: 979–986. doi: 10.1139/E2012-015.

Godin, E., Fortier, D., and Coulombe, S. 2014. Effects of thermo-erosion gullying on hydrologic flow networks, discharge and soil loss. Environ. Res. Lett. **9**(10). doi: 10.1088/1748-9326/9/10/105010.

Godin, E., Fortier, D., and Lévesque, E. 2016. Nonlinear thermal and moisture response of ice-wedge polygons to permafrost disturbance increases heterogeneity of high Arctic wetland. Biogeosciences. **13**: 1439–1452. doi: 10.5194/bg-13-1439-2016.

Goward, S.N., Davis, P.E., Fleming, D., Miller, L., and Townshend, J.R. 2003. Empirical comparison of Landsat 7 and IKONOS multispectral measurements for selected Earth Observation System (EOS) validation sites. Remote Sens. Environ. **88**: 80–99. doi: 10.1016/j.rse.2003.07.009.

Grosse, G., Harden, J., Turetsky, M., McGuire, A.D., Camill, P., Tarnocai, C., Frolking, S., Schuur, E.A.G., Jorgenson, T., et al. 2011. Vulnerability of high-latitude soil organic carbon in North America to disturbance. J. Geophys. Res. **116**: G00K06, doi: 10.1029/2010JG001507.

Günther, F., Overduin, P.P., Sandakov, A.V., Grosse, G., and Grigoriev, M.N. 2013. Short- and long-term thermo-erosion of ice-rich permafrost coasts in the Laptev Sea region. Biogeosciences. **10**: 4297–4318. doi: 10.5194/bg-10-4297-2013.

Günther, F., Overduin, P.P., Yakshina, I.A., Opel, T., Baranskaya, A.V., and Grigoriev, M.N. 2015. Observing Muostakh disappear: permafrost thaw subsidence and erosion of a ground-ice-rich island in response to arctic summer warming and sea ice reduction. Cryosphere. **9**: 151–178. doi: 10.5194/tc-9-151-2015.

Hansen, R.R., Hansen, O.L.P., Bowden, J.J., Treier, U.A., Normand, S., and Høye, T. 2016. Meter scale variation in shrub dominance and soil moisture structure Arctic arthropod communities. PeerJ. **4**: e2224, doi: 10.7717/peerj.2224.

Henry, G.H.R. 1998. Environmental influences on the structure of sedge meadows in the Canadian High Arctic. Plant Ecol. **134**: 119–129.

Hubbard, S.S., Gangodagamage, C., Dafflon, B., Wainwright, H., Peterson, J., Gusmeroli, A., Ulrich, C., Wu, Y., Wilson, C., and Rowland, J. 2013. Quantifying and relating land-surface and subsurface variability in permafrost environments using LiDAR and surface geophysical datasets. Hydrogeol. J. **21**: 149–169. doi: 10.1007/s10040-012-0939-y.

Hugelius, G., Strauss, J., Zubrzycki, S., Harden, J.W., Schuur, E.A.G., Ping, C.-L., Schirrmeister, L., Grosse, G., Michaelson, G.J., et al. 2014. Estimated stocks of circumpolar permafrost carbon with quantified uncertainty ranges and identified data gaps. Biogeosciences. **11**: 6573–6593. doi: 10.5194/bg-11-6573-2014.
Hughes, R.J., Reed, A., and Gauthier, G. 1994. Space and habitat use by greater snow goose broods on Bylot Island, Northwest Territories. J. Wildlife Manage. **58**: 536–545. doi: 10.2307/3809326.
Inland Waters Branch. 1969. Glacier atlas of Canada, Bylot Island area, 46201. Inland Waters Branch, Environment Canada, Ottawa, Ont.
Jorgenson, M.T., and Grosse, G. 2016. Remote sensing of landscape change in permafrost regions. Permafrost Periglac. **27**: 324–338. doi: 10.1002/ppp.1914.
Jorgenson, M.T., Shur, Y.T., and Pullman, E.R. 2006. Abrupt increase in permafrost degradation in Arctic Alaska. Geophys. Res. Lett. **33**: L02503, doi: 10.1029/2005GRL024960.
Kanevskiy, M., Shur, Y., Jorgenson, M.T., Ping, C.L., Michaelson, G.J., Fortier, D., Stephani, E., Dillon, M., and Tumskoy, V. 2013. Ground ice in the upper permafrost of the Beaufort Sea coast of Alaska. Cold Reg. Sci. Technol. **85**: 56–70. doi: 10.1016/j.coldregions.2012.08.002.
Klein, E., Berg, E.E., and Dial, R. 2005. Wetland drying and succession across the Kenai Peninsula Lowlands, south-central Alaska. Can. J. For. Res. **35**: 1931–1941. doi: 10.1139/X05-129.
Kokelj, S.V., and Jorgenson, M.T. 2013. Advances in thermokarst research. Permafrost Periglac. **24**: 108–119. doi: 10.1002/ppp.1779.
Kokelj, S.V., Lantz, T.C., Wolfe, S.A., Kanigan, J.C., Morse, P.D., Coutts, R., Molina-Giraldo, N., and Burn, C.R. 2014. Distribution and activity of ice wedges across the forest–tundra transition, western Arctic Canada. J. Geophys. Res. Earth Surf. **119**: 2032–2047. doi: 10.1002/2014JF003085.
Kristensen, D.K., Kristensen, E., Forchhammer, M.C., Michelsen, A., and Schmidt, N.M. 2011. Arctic herbivore diet can be inferred from stable isotopes in C_3 plants, faeces, and wool. Can. J. Zool. **89**: 982–899. doi: 10.1139/Z11-073.
Laidler, G.J., and Treitz, P. 2003. Biophysical remote sensing of arctic environments. Prog. Phys. Geog. **27**: 44–68. doi: 10.1191/0309133303pp358ra.
Laidler, G.J., Treitz, P., and Atkinson, D.M. 2008. Remote sensing of Arctic vegetation: relations between the NDVI, spatial resolution and vegetation cover on Boothia Peninsula, Nunavut. Arctic. **61**: 1–13. doi: 10.14430/arctic2.
Lantz, T.C., Kokelj, S.V., and Fraser, R.H. 2015. Ecological recovery in an Arctic delta following widespread saline incursion. Ecol. Appl. **25**: 172–185. doi: 10.1890/14-0239.1.
Lecomte, N., Gauthier, G., and Giroux, J.-F. 2008. Breeding dispersal in a heterogeneous landscape: the influence of habitat and nesting success in greater snow goose. Oecologia. **155**: 33–41. doi: 10.1007/s00442-007-0860-6.
Legagneux, P., Gauthier, G., Berteaux, D., Bêty, J., Cadieux, M.-C., Bilodeau, F., Bolduc, E., McKinnon, L., Tarroux, A., et al. 2012. Disentangling trophic relationships in a High Arctic tundra ecosystem through food web modeling. Ecology. **93**: 1707–1716. doi: 10.1890/11-1973.1.
Lepage, D., Nettleship, D.N., and Reed, A. 1998. Birds of Bylot Island and adjacent Baffin Island, Northwest Territories, Canada, 1979 to 1997. Arctic. **51**: 125–141. doi: 10.14430/arctic1054.
Levy, J.S., Head, J.W., and Marchant, D.R. 2008. The role of thermal contraction crack polygons in cold-desert fluvial systems. Antarct. Sci. **20**: 565–579. doi: 10.1017/S0954102008001375.
Liljedahl, A.K., Hinzman, L.D., and Schulla, J. 2012. Ice-wedge polygon type controls low-gradient watershed-scale hydrology. *In* Proceedings, Tenth International Conference on Permafrost (TICOP), Salekhard, Russia.
Liljedahl, A.K., Boike, J., Daanen, R.P., Fedorov, A.N., Frost, G.V., Grosse, G., Hinzman, L.D., Iijma, Y., Jorgenson, J.C., et al. 2016. Pan-Arctic ice-wedge degradation in warming permafrost and its influence on tundra hydrology. Nature Geosci. **9**: 312–318. doi: 10.1038/ngeo2674.
Liu, L., Jafarov, E.E., Schaefer, K.M., Jones, B.M., Zebker, H.A., Williams, C.A., Rogan, J., and Zhang, T. 2014. InSAR detects increase in surface subsidence caused by an Arctic tundra fire. Geophys. Res. Lett. **41**: 3906–3913. doi: 10.1002/L060533.
Liu, L., Schaefer, K.M., Chen, A.C., Gusmeroli, A., Zebker, H.A., and Zhang, T. 2015. Remote sensing measurements of thermokarst subsidence using InSAR. J. Geophys. Res. Earth Surf. **120**: 1935–1948. doi: 10.1002/2015JF003599.
Massé, H. 1998. Estimation de la capacité de support des différents écosystèmes humides utilisés par la grande oie des neiges nichant à l'île Bylot (Nunavut, Canada). M.Sc. thesis, Université Laval, Québec, Qué.
McEwing, K.R., Fisher, J.P., and Zona, D. 2015. Environmental and vegetation controls on the spatial variability of CH_4 emission from wet-sedges and tussock tundra ecosystems in the Arctic. Plant Soil. **338**: 37–52. doi: 10.1007/s11104-014-2377-1.
Morgenstern, A. 2012. Thermokarst and thermal erosion: degradation of Siberian ice-rich permafrost. Ph.D. thesis, University of Potsdam, Potsdam, Germany.
Morgenstern, A., Ulrich, M., Günther, F., Roessler, S., Fedorova, I.V., Rudaya, N.A., Wetterich, S., Boike, J., and Schirrmeister, L. 2013. Evolution of thermokarst in East Siberian ice-rich permafrost: a case study. Geomorphology. **201**: 363–379.
Muster, S., Heim, B., Abnizova, A., and Boike, J. 2013. Water body distributions across scales: a remote sensing based comparisons of three Arctic tundra wetlands. Remote Sens. **5**: 1498–1523. doi: 10.3390/rs5041498.
Natali, S.M., Schuur, E.A.G., Mauritz, M., Schade, J.D., Celis, G., Crummer, K.G., Johnston, C., Krapek, J., Pegoraro, E., et al. 2015. Permafrost thaw and soil moisture driving CO_2 and CH_4 release from upland tundra. J. Geophys. Res. Biogeosci. **120**: 1–13. doi: 10.1002/2014JG002872.
Obu, J., Lantuit, H., Fritz, M., Pollard, W.H., Sachs, T., and Günther, F. 2016. Relation between planimetric and volumetric measurements of permafrost coast erosion: a case study from Herschel Island, western Canadian Arctic. Polar Res. **35**(1): 30313, doi: 10.3402/polar.v35.30313.

Olefeldt, D., Turetsky, M.R., Crill, P.M., and McGuire, A.D. 2013. Environmental and physical controls on northern terrestrial methane emissions across permafrost zones. Glob. Change Biol. **19**: 589–603. doi: 10.1111/gcb.12071.

Park, T., Ganguly, S., Tømmervik, H., Euskirchen, E.S., Høgda, K.-A., Karlsen, S.R., Brovkin, V., Nemani, R.R., and Myneni, R.B. 2016. Changes in growing season duration and productivity of northern vegetation inferred from long-term remote sensing data. Environ. Res. Lett. **11**: 084004, doi: 10.1088/1748-9326/11/8/084001.

Pattison, R.R., Jorgenson, J.C., Raynolds, M.K., and Welker, J.M. 2015. Trends in NDVI and tundra community composition in the Arctic of NE Alaska between 1984 and 2009. Ecosystems. **18**: 707–719. doi: 10.1007/s10021-015-9858-9.

Perreault, N. 2012. Impact de la formation de ravins de thermo-érosion sur les milieux humides, Ile Bylot, Nunavut, Canada. M.Sc. thesis, Université du Québec à Trois-Rivières, Trois-Rivières, Qué.

Perreault, N., Lévesque, E., Fortier, D., and Lamarque, L.J. 2016. Thermo-erosion gullies boost the transition from wet to mesic tundra vegetation. Biogeosciences. **13**: 1237–1253. doi: 10.5194/bg-13-1237-2016.

Pettorelli, N. 2013. The normalized difference vegetation index. Oxford University Press, Oxford, UK.

Pienitz, R., Doran, P.T., and Lamoureux, S.F. 2008. Origin and geomorphology of lakes in the polar regions. *In* Polar lakes and rivers, limnology of Arctic and Antarctic aquatic ecosystems. *Edited by* W.F. Vincent and J. Laybourn-Parry. Oxford University Press, Oxford, UK. pp. 25–41.

Pouliot, R., Rochefort, L., and Gauthier, G. 2009. Moss carpets constrain the fertilizing effects of herbivores on graminoid plants in arctic polygon fens. Botany. **87**: 1209–1222. doi: 10.1139/B09-069.

Rautio, M., Dufresne, F., Laurion, I., Bonilla, S., Vincent, W.F., and Christoffersen, K.S. 2011. Shallow freshwater ecosystems of the circumpolar Arctic. Ecoscience. **18**: 204–222. doi: 10.2980/18-3-3463.

Raynolds, M.K., and Walker, D.A. 2009. Effects of deglaciation on circumpolar distribution of arctic vegetation. Can. J. Remote Sens. **35**: 118–129. doi: 10.5589/m09-006.

Raynolds, M.K., Comiso, J.C., Walker, D.A., and Verbyla, D. 2008. Relationship between satellite-derived land surface temperatures, arctic vegetation types, and NDVI. Remote Sens. Environ. **112**: 1884–1894.

Riedel, S.M., Epstein, H.E., Walker, D.A., Richardson, D.L., Calef, M.P., Edwards, E., and Moody, A. 2005. Spatial and temporal heterogeneity of vegetation properties among four tundra plant communities at Ivotuk, Alaska, U.S.A. Arct. Antarct. Alp. Res. **37**: 25–33. doi: 10.1657/1523-0430(2005)037[0025:SATHOV]2.0.CO;2.

Romanovsky, V.E., Smith, S.L., and Christiansen, H.H. 2010. Permafrost thermal state in the polar Northern Hemisphere during the international polar year 2007–2009: a synthesis. Permafrost Periglac. **21**: 106–116. doi: 10.1002/ppp.689.

Rongqun, Z., and Daolin, Z. 2011. Study of land cover classification based on knowledge rules using high-resolution remote sensing images. Expert Syst. Appl. **38**: 3647–3652. doi: 10.1016/j.eswa.2010.09.019.

Rouse, J.W., Haas, R.H., Schell, J.A., and Deering, D.W. 1973. Monitoring vegetation systems in the Great Plains with ERTS. *In* 3rd ERTS Symposium, NASA SP-351. Vol. 1. pp. 309–317.

Rowland, J.C., Jones, C.E., Altmann, G., Bryan, B., Crosby, B.T., Geernaert, G.L., Hinzman, L.D., Kane, D.L., Lawrence, D.M., et al. 2010. Arctic landscapes in transition: responses to thawing permafrost. Eos Trans. Am. Geophys. Union. **91**: 229–236. doi: 10.1029/2010EO260001.

Rudy, A.C.A., Lamoureux, S.F., Treitz, P., and Collingwood, A. 2013. Identifying permafrost slope disturbance using multi-temporal optical satellite images and change detection techniques. Cold Reg. Sci. Technol. **88**: 37–49. doi: 10.1016/j.coldregions.2012.12.008.

Rudy, A.C.A., Lamoureux, S.F., Treitz, P., Van Ewijk, K., Bonnaventure, P.P., and Budkewitsch, S. 2017. Terrain controls and landscape-scale modelling of active-layer detachments, Sabine Peninsula, Melville Island, Nunavut. Permafrost Periglac. **28**: 79–91. doi: 10.1002/ppp/1900.

Saruulzaya, A., Ishikawa, M., and Jambaljav, Y. 2016. Thermokarst lake changes in the southern fringe of Siberian permafrost region in Mongolia using Corona, Landsat, and ALOS satellite imagery from 1962 to 2007. Adv. Remote Sens. **5**: 215–231. doi: 10.4236/ars.2016.54018.

Schaefer, K., Liu, L., Parsekian, A., Jafarov, E., Chen, A., Zhang, T., Gusmeroli, A., Panda, S., Zebker, H.A., and Schaefer, T. 2015. Remotely sensed active layer thickness (ReSALT) at Barrow, Alaska using interferometric synthetic aperture radar. Remote Sens. **7**: 3735–3759. doi: 10.3390/rs70403735.

Skurikhin, A.N., Gangodagamage, C., Rowland, J.C., and Wilson, C.J. 2013. Arctic tundra ice-wedge landscape characterization by active contours without edges and structural analysis using high-resolution satellite imagery. Remote Sens. Lett. **4**: 1077–1086. doi: 10.1080/2150704X.2013.840404.

Stow, D.A., Hope, A., McGuire, D., Verbyla, D., Gamon, J., Huemmrich, F., Houston, S., Racine, C., Sturm, M., et al. 2004. Remote sensing of vegetation and land-cover change in Arctic tundra ecosystems. Remote Sens. Environ. **89**: 281–308. doi: 10.1016/j.rse.2003.10.018.

Tarnocai, C., Canadell, J.G., Schuur, E.A.G., Kuhry, P., Mazhitova, G., and Zimov, S. 2009. Soil organic carbon pools in the northern circumpolar permafrost region. Glob. Biochem. Cycles. **23**: GB2023, doi: 10.1029/2008GB003327.

Thomas, V., Treitz, P., Jelinski, D., Miller, J., Lafleur, P., and McCaughney, J.H. 2003. Image classification of a northern peatland complex using spectral and plant community data. Remote Sens. Environ. **84**: 83–99. doi: 10.1016/S0034-4257(02)00099-8.

Treat, C.C., Natali, S.M., Ernakovitch, J., Iversen, C.M., Lupascu, M., McGuire, A.D., Norby, R.J., Chowdhury, T.R., Richter, A., and Santruckova, H. 2015. A pan-Arctic synthesis of CH_4 and CO_2 production from anoxic soil incubations. Glob. Change Biol. **21**: 2787–2803. doi: 10.1111/gcb.12875.

Tucker, C.J., and Sellers, P.J. 1986. Satellite remote sensing of primary production. Int. J. Remote Sens. **7**: 1395–1416

Turner, D., Lucieer, A., and de Jong, S.M. 2015. Time series analysis of landslide dynamics using an Unmanned Aerial Vehicle (UAV). Remote Sens. **7**: 1736–1757. doi: 10.3390/rs70201736.

Tveit, A.T., Urich, T., Frenzel, P., and Svenning, M.M. 2015. Metabolic and trophic interactions modulate methane production by Arctic peat microbiota in response to warming. Proc. Natl. Acad. Sci. U.S.A. **112**: E2507–E2516. doi: 10.1073/pnas.1420797112.

Ulrich, M., Grosse, G., Strauss, J., and Schirrmeister, L. 2014. Quantifying wedge-ice volumes in yedoma and thermokarst basin deposits. Permafrost Periglac. **25**: 151–161. doi: 10.1002/ppp.1810.

Veillette, A., Fortier, D., and Godin, E. 2015. Contrasting patterns of thermo-erosion gullies formed in syngenetic ice wedge polygonal terrains on Bylot Island, Nunavut, eastern Canadian Arctic: case studies from three different sedimentary environments. *In* 68th Canadian Geotechnical Conference and 7th Canadian Permafrost Conference, Quebec City, Que.

Vincent, W., Lemay, M., and Allard, M. 2017. Arctic permafrost landscapes in transition: towards an integrated Earth system approach. Arct. Sci. **3**: This issue.

Vonk, J.E., Mann, P.J., Dowdy, K.L., Davydova, A., Davydov, S.P., Zimov, N., Spencer, R.G.M., Bulygina, E.B., Eglinton, T.I., and Holmes, R.M. 2013. Dissolved organic carbon loss from yedoma permafrost amplified by ice wedge thaw. Environ. Res. Lett. **8**: 035023, doi: 10.1088/1748-9326/8/3/035023.

Widhalm, B., Bartsch, A., Leibman, M., and Khomutov, A. 2017. Active-layer thickness estimation from X-band SAR backscatter intensity. Cryosphere. **11**: 483–496. doi: 10.5194/tc-11-483-2017.

Wolfe, S.A., Short, N.H., Morse, P.D., Schwarz, S.H., and Stevens, C.W. 2014. Evaluation of RADARSAT-2 DInSAR seasonal surface displacement in discontinuous permafrost terrain, Yellowknife, Northwest Territories, Canada. Can. J. Remote Sens. **40**: 406–422. doi: 10.1080/07038992.2014.1012836.

Woo, M.-K. 2012. Permafrost hydrology. Springer, New York.

Wrona, F.J., Johansson, M., Culp, J.M., Jenkins, A., Mård, J., Myers-Smith, I.H., Prowse, T.D., Vincent, W.F., and Wookey, P.A. 2016. Transitions in Arctic ecosystems: ecological implications of a changing hydrological regime. J. Geophys. Res. Biogeosci. **121**: 650–674. doi: 10.1002/2015JG003133.

Zoltai, S.C., McCormick, K.J., and Scotter, G.W. 1983. A natural resource survey of Bylot Island and adjacent Baffin Island, Northwest Territories. Parks Canada, Ottawa, Ont.